THESIS

CHARACTERIZING CANINE DOSE FROM EXTERNAL BEAM IRRADIATION

Submitted by

Cheri Nichole Hall

Department of Environmental and Radiological Health Sciences

In partial fulfillment of the requirements

For the Degree of Master of Science

Colorado State University

Fort Collins, Colorado

Summer 2011

Master's Committee:

Advisor: Thomas Johnson

Anna Dee Fails
Elissa Randall

ABSTRACT

CHARACTERIZING CANINE DOSE FROM EXTERNAL BEAM IRRADIATION

Absorbed dose from Computed Tomography (CT) is a major concern on an individual basis as well as for the collective population due to increased frequency of and dependency on CT scans for diagnostic and therapeutic imaging. Colorado State University recently integrated a large bore multi-slice Positron Emission Tomography and Computed Tomography (PET/CT) scanner into the Veterinary Teaching Hospital. The new PET/CT and high volume of canine CT imaging exams provides a unique opportunity for research into canine organ dose that compliments efforts aimed at characterizing human CT dose. This retrospective study focuses on characterizing the internal dose to a canine brain from a CT scan to a canine body. Organ specific doses were directly measured using an ion chamber placed within a physical canine anatomic phantom. Since dogs have been shown to be a valuable translational model for human radiation effects, accurate estimation of canine CT dose may permit future deterministic and stochastic radiobiological effect studies to be performed with canines on a much shorter time scale than similar studies with humans.

Equivalent doses were calculated with a mean (± standard deviation) of 12.96 (± 0.45) mSv, 32.80 (± 0.77) mSv, and 49.24 (± 0.87) mSv for 90, 120 and 140 kVp respectively at a fixed 300 mAs in the brain of the canine phantom. Additionally, these data were fit to a parallel set of human expected doses to the brain of a ten year old child and an adult. The dog data was found to be a good fit to the child data. It was concluded that a dog most closely fits a ten year old child for dose comparisons from CT procedures. The dose comparisons from scattered radiation

require more data collection and analysis to best characterize the relationship. Preliminary analysis of scattered radiation to the brain from a chest scan also indicates the child is the best fit for a dose comparison with the canine phantom.

ACKNOWLEDGEMENTS

I would like to acknowledge my committee Dr. Thomas Johnson, Dr. Elissa Randall and Dr. Anna Fails without whose support I could not have completed this project.

I would also like to acknowledge Billie Arceneaux, Dr. Fred Harmon, Dr. John Pinder, Jim Self, Dr. James Winslow, Dr. Colleen Duncan, Dr. Bob Wilson, the guys at UWM-RCL, and many others who stepped in to fill voids and give guidance when I was most desperate.

I would like to thank the Mountains and Plains Education and Resource Center for financial support and a plethora of experiences during the completion of this degree.

To new friends and old, family and foes: you make my life meaningful. You give me the strength and purpose necessary to be the best version of myself. I would like to thank and acknowledge each of you for the role you have had in my life and allowing me to be part of yours.

DEDICATION

To H07233-ED7:

While no one may ever know your name, you will always be my Legacy.

TABLE OF CONTENTS

CHAPTER 1

INTRODUCTION

1.1 Medical imaging impacts average American dose

The American population is exposed to ionizing radiation from a variety of sources, and these sources were evaluated and quantified by the National Council on Radiation Protection and Measurements (NCRP) in Report No. 160 for the US population in 2006. Exposures were separated in five broad categories: ubiquitous background; medical procedures; consumer products or activities; industrial, security, medical, educational and research sources; and occupational exposures [1]. Medical imaging includes computed tomography (CT), nuclear medicine (positron emission tomography; PET), interventional fluoroscopy, external-beam radiotherapy, and conventional radiography and fluoroscopy. Each imaging modality presents unique radiation risks and benefits to patients but adds to the overall radiation dose to the United States general population. Computed Tomography contributes a large portion of the total dose to the population due to the design of the imaging instrument, motivation for and degree of use in the United States, and the specific dose contributions from CT.

Computed Tomography utilizes x-ray technology and computing power to reconstruct three-dimensional images of objects. A thin beam of x-rays is passed through an object from multiple angles and detected 180 degrees from the x-ray source. The number of photons attenuated is related to atomic characteristics and densities of the object. The computer uses the signal detected to backproject the areas of highest intensity of photons, or lowest attenuation, and

through a digital algorithm, produces a cross-sectional image of the object [2]. All of these cross-sections (slices) are assembled to give a 3-D view. CT gives an anatomical view into the body that was once only available through exploratory surgery [2]. Many diseases are more easily detected and treated through the advances of CT imaging. The utility of CT scans spurred the prevalent use in clinical settings.

There are numerous parameters that characterize a CT scan. Parameters vary with imaging techniques to alter the quality of the image. Each CT parameter can affect the dose to the patient independently but often the parameters are altered in conjunction with one another. In general, the radiation exposure increases with the need for greater image resolution.

A major contributor to radiation dose from CT is pitch, which is a measure of the number of rotations of the x-ray source around the body per unit length of the body, and is a measure of the coverage of an object being scanned. Pitch is a useful descriptor when operating a helical scanner. The pitch is defined according to the type of scanner in use. For a single detector array the collimation pitch is defined as the table movement in mm per 360-degree rotation divided by the collimator width in mm at the isocenter. In this setting a pitch of 1.0 is equivalent to contiguous axial scans while less than 1.0 results in overlap of the beam and more than 1.0 is partial scanning. The definition changes slightly when using a multi-detector array. In both instances, however, the pitch impacts the dose to the patient due to the nature of increasing or decreasing the number of rotations required to cover the same area of the patient. A higher pitch results in a lesser dose. A lower pitch results in a greater dose since the rotations overlap and result in multiple radiation exposures to each cross-section of the body. The benefit of a lower pitch is higher resolution [2]. Pitch also impacts the time required to complete imaging, with a higher pitch resulting in shorter scan times.

As with pitch, slice thickness can significantly impact dose, scan times, and image quality. Transverse slice thicknesses vary greatly and depend on the detector size and beam collimation. For multiple detector arrays, the dose per slice is increased as the slice thickness decreases [2]. Increased slice thickness decreases spatial resolution but increases contrast resolution [2]. Dose is also increased due to necessary adjustments in the collimation that keeps the beam in line with the detectors. Collimation causes the penumbra to fall outside the detectors and add to the overall dose. Collimators are lead shields that determine the size and shape of the x-ray beam projected from the tube. Ultimately, collimation determines the detector combination used for multi-detector arrays.

Tube current characterizes the stream of electrons accelerating from the cathode to impact the high density anode target (usually made of tungsten). The tube current is measured in milliamps (mA) and often combined with the scan time in seconds (s). The effects on dose from the mAs are linear and dose can be scaled in relation to mAs. As mAs increases, the number of photons passing through the patient increases resulting in a larger dose but leads to better contrast resolution in the image.

The potential difference between the cathode and the anode in the x-ray tube is described in volts (V). The energy gained by the electrons accelerated through this potential is proportional to the potential difference, and the energy released in the form of x-rays is directly linked to the energy of the electron. The kilovolt peak (kVp) is used to describe the difference applied across the tube and thereby the maximum energy of the x-rays produced. The energy of the x-rays directly impact patient dose. As the energy of the x-rays increases, the dose to the patient increases. Contrast decreases with greater kVp, but higher voltages are necessary to image larger patients as the energy necessary to pass through the patient increases.

The ability of the detector to identify incident photons then translate them to signals for the computer to create the images is called the detector efficiency. If the efficiency is low, more photons are required to produce the same image and the dose is increased. Similar to detector efficiency is geometric efficiency, which is dependent on the geometric relationship between the source and the detector [2]. Both types of efficiencies are inherent to the instrument and cannot be controlled by the operator.

Variability among CT instruments and protocols is an important contributor to dose. Differences of 2 – 40 times the dose in human medicine have been reported between different CT facilities [3-4]. While some of this is due to instrument variability in collimation, filtration, detector efficiency or geometry, the majority of the differences are due to techniques chosen by the operator [4-5]. Strict protocols can reduce dose variability.

Computed Tomography imaging uses low energy x-rays. X-rays, or photons, are low linear energy transfer (low LET) radiation. As photons pass through a cell, the amount of energy deposited per unit length is low compared to other types of ionizing radiation such as alpha or high z particles [2]. Background radiation, especially cosmic radiation, is generally high energy and high LET resulting in higher doses and a greater cell damage and genetic impact [1-2].

The benefits of CT over conventional radiography lend CT to be useful in a multitude of clinical settings as a diagnostic tool. One benefit is an increased sensitivity of the detectors in CT to the x-ray attenuation spectrum, which allows for a more detailed image of the tissues present. A second benefit is the reduction in tissue averaging due to an overlap of tissue. In a CT image, the tissue cross-section is much thinner than conventional radiography; therefore, a single photon does not have to travel through as much tissue and is a better estimate of the density of the tissue at a particular point. As a consequence of its utility, the use of CT in clinical

settings has increased approximately 8 to 15% from the previous year over the last 7 to 10 years [1].

While modern multi-detector CT (MDCT) scanners have the capability to reduce dose due to the increased speed and efficiency over single detector scanners, these advances augment the demand for the use of CT scans in everyday practice resulting in a higher collective effective dose (*S*) to the U.S. population [1]. Collective dose is defined as the sum of all the effective doses to individuals in a population resulting in the total dose to the population, given in person-Sieverts (person-Sv). Collective dose can also be calculated as the product of the mean effective dose (E_{pop}) for an individual in a population and the number of people in that population [1].

NCRP 160 characterized the total number of CT procedures performed in 2006 by utilizing multiple databases around the United States including IMV, Medicare, U.S. Department of Veterans Affairs, Large National Employer Plan (LNEP), and commercial sources. The total number of CT procedures was estimated to be about 62 million which was approximately an 8% increase over the previous year [1]. However, Medicare data showed that a number of these procedures included two scans for the use of contrast. By using the Medicare data, NCRP estimated the total number of scans to be closer to 67 million for 2006 [1]. NCRP also reported an average of approximately a 10 to 11 percent increase per year from 1993 to 2006 [1], indicating if the trend persisted at only an 8 % increase per year since 2006 the estimated number of scans in 2011 is about 98 million scans.

Medical exposure accounts for forty-eight percent of the overall collective dose (S) or the effective dose per individual (E_{us}) in the United State [1]. Out of the overall S, the total collective dose from medical exposure has increased by a factor of 7.3 to a total of 899,000 person–Sv since 1980. A portion of this is due to the population increase of thirty percent. However, the effective dose per individual (E_{us}), which accounts for the change in population, increased by a

factor of 5.7 from 1980 to 2006 resulting in a E_{us} of 3 mSv from medical exposures. Of this E_{us}, forty-nine percent is from computed tomography [1]. In Figure 1 and 2, a resulting twenty-four percent of the overall S and E_{us}, and 50% of the dose from medical come from CT. A more detailed view of the values contributing to S and E_{us} are shown in Table 1 in the appendix.

As evident in Figure 2, the U.S. population is exposed to two major sources of ionizing radiation: ubiquitous background radiation and medical exposure to patients. The largest source of medical exposure is from computed tomography. While each source of radiation has an associated risk, CT with its high clinical demand, low energy x-rays and the uncertainty surrounding the effects of low doses is an area of risk that needs to be further examined and characterized.

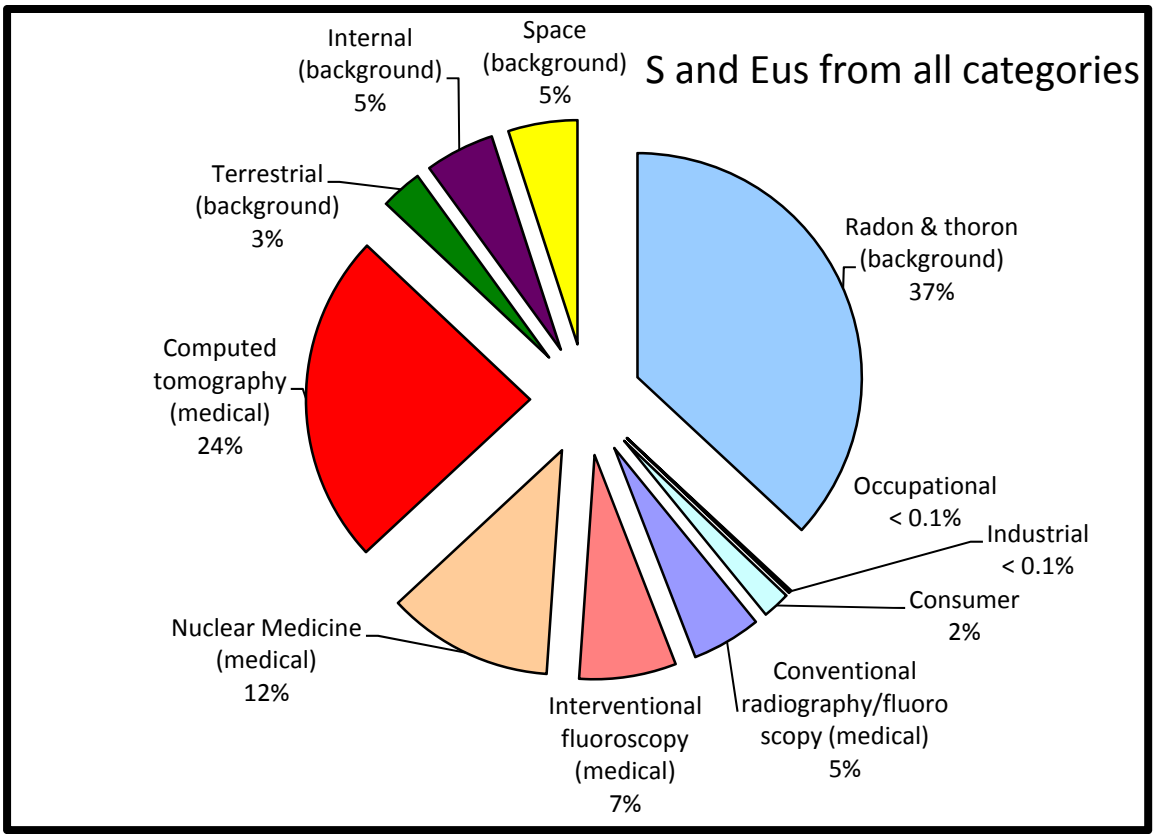

Figure 1. Percentages from major contributors to the overall collective dose (S) and effective dose (E_{us}) to the U.S. population. Data adapted from NCRP 160 [1].

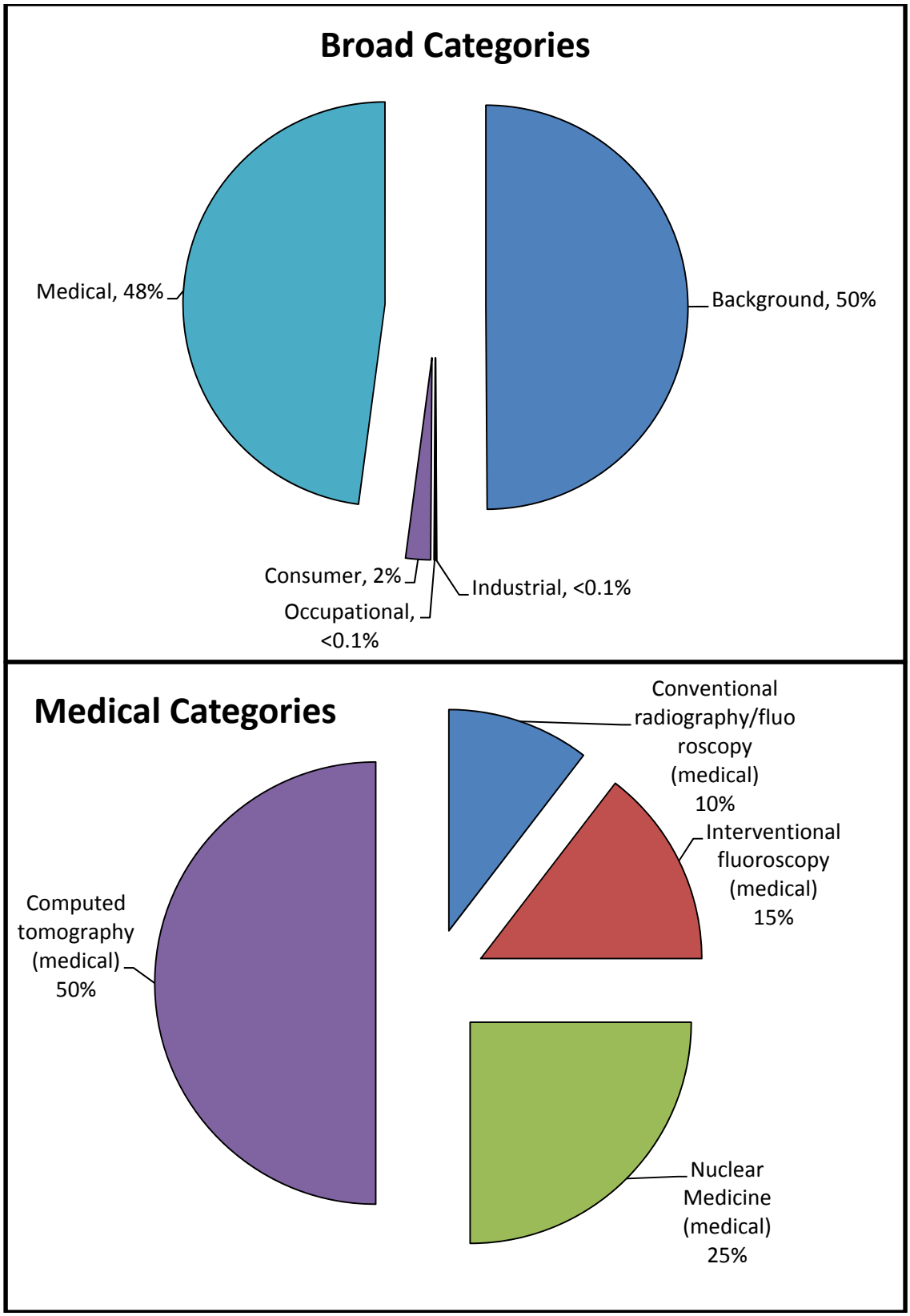

Figure 2 – Percent contributions to S and E_{us} from ionizing radiation due to the broad categories, and contributions broken down in the medical category. Data adopted from NCRP 160 [1].

Damage from radiation induces two categories of effects: stochastic and non-stochastic (or deterministic) effects. A threshold dose must be exceeded to result in deterministic effects [6]. The threshold doses typically associated with deterministic effects are greater than those seen in CT imaging [6]. The major concern from low doses of radiation is stochastic effects. Stochastic effects are hypothesized to occur without a threshold level. Stochastic effects are generally characterized by probability, which is proportional to the dose. Stochastic effects are not characterized by severity, which is independent of dose. Cancer and genetic effects are considered stochastic effects [7].

1.2 BEIR VII Report - Linear No Threshold

The Biological Effects of Ionizing Radiation (BEIR) VII committee

> "concludes that current scientific evidence is consistent with the hypothesis that there is a linear dose-response relationship between exposure to ionizing radiation and the development of radiation-induced solid cancers in humans. The committee further judges it unlikely that a threshold exists for the induction of cancers at low doses will be small [8]."

The Lifetime Survival Study (LSS) was used to estimate lifetime risks of cancer and was adjusted to fit the U.S. population. When the data was fit to the U.S. population, uncertainties were acknowledged including the "possible reduction in risk for exposure at low doses and low dose rates [8]." After further evaluation, the BEIR committee decided the linear risk estimates at low doses or low dose rates should be reduced by a factor of 1.1 to 2.3 [8]. However, the BEIR committee maintains the linear dose-response relationship for solid cancers in humans and concludes it is unlikely that a threshold exists. The BEIR VII committee does concur that the risk of cancer at small doses poses a low risk of radiation-induced cancer. The BEIR committee had insufficient data to make assessments on other health effects (i.e. heart disease or stroke) at

low doses of radiation, and holds that while no heritable diseases have presented in humans due to ionizing radiation, the risk still may exist as it has been seen in other organisms [8].

1.3 Benefits and Applicability of the Canine Species as a Model

The first commercial PET/CT dedicated to veterinary medicine in the United States was recently installed at Colorado State University's James L. Ross Veterinary Teaching Hospital (VTH). The GEMINI TruFlight Big Bore PET/CT from Phillips Healthcare is frequently used in conjunction with the Varian Trilogy linear accelerator the Colorado State University Animal Cancer Center (ACC) uses for cancer treatment.

Advances in cancer detection and treatment, as well as numerous other diseases, have been made using the PET/CT technology. The scanner consists of a CT bore that provides anatomic data as 3-D images, followed by a PET bore that provides physiologic data. Positron Emission Tomography (PET) operates using principles of coincident detection. PET requires a radioactive substance be injected into the patient and the emissions are detected by the PET scanner. The additional dose from PET requires a unique method of dosimetry. The theory of PET and dose due to PET are not part of this study.

Beside the direct benefit of this installation to the patients of the VTH, the innovative technology of PET/CT in a veterinary setting provides opportunities for research into animal exposure and cancers that compliment efforts in human research. Cancer and genetic effects take a significant amount of time to develop in humans and therefore it would be useful to find a method that will demonstrate the impacts of radiation on living organisms on a shorter time scale. A canine model has been proposed as suitable for such studies.

In 2008, the National Cancer Institute held a meeting entitled 'Translation of new cancer treatments from canine to human cancer patients.' The meeting focused on how to best use dogs for cancer treatment studies. One of the reasons given to choose the canine species was

the “naturally occurring tumors in dogs share many clinical and molecular similarities to human cancers [9].” These tumors occur spontaneously in the dog’s life similar to human cancers.

Animals have been used to test theories in genetic, surgical, cancer, and numerous other types of research dating back to the 2nd century [10]. Research animals replaced or preceded human testing and served a crucial role in furthering the understanding of biological systems, genetics, and medicine. The canine species is reported to exhibit over 450 diseases of which about 360 are analogous to human diseases [11]. The domestic dog has proven particularly useful in understanding cancer development and in treatment studies due to a variety of factors. With more than one million dogs diagnosed with cancer annually [12], the canine species is readily available for research as most owners are willing to consent to place their dogs in studies [13]. Factors that make pet dogs ideal for research are the compressed lifespan [13-14](normative value of 12 years [15]) and similarities in biokinetics with relation to metabolism of drugs and cell kinetics [13, 16].

For many diseases the latency period, which is the amount of time from exposure to a hazard until a deleterious effect manifests, for humans is long. A long latency period makes it difficult to perform timely research and allows more opportunity for the subject to be exposed to a large number of hazards that could cause the same effects. It has been noted in many situations that the latency period for dogs is much shorter than in humans. A striking example is that of mesothelioma. It is well know through epidemiologic studies that asbestos exposure can lead to mesothelioma in humans. Studies also show a link between pet owners, whose occupation or hobby are asbestos related, and the development of mesothelioma in the pet dogs. With a much shorter latency period of 8 years between exposure and cancer development opposed to the average 30 years for humans [13], a companion animal offers many opportunities to better understand both the causes and the development of diseases in a more

time efficient manner. Other examples include osteosarcoma and lymphoma with latency periods of 18 months for dogs and 7 years for humans [12].

Scientific advances have provided a better understanding of canine genetics and shown stronger similarities between canine and human genetics than human and rodent [14, 16]. Detailed examinations into cancer histologies demonstrate similarities between dogs and humans [16]. The array of genetic material and the variety of types of cancer seen among canine breeds are mirrored in the diverse genetic pool of human races [12, 16]. As the majority of radiation-induced mutations are DNA related, similarities in genetic make-up are crucial to produce the same alterations from ionizing radiation. Unsurprisingly, there are examples of human cancer contributors being present in the corresponding canine cancer. Instances exist where identical tumor oncogenes and tumor suppressors are present in both canine and human variations of the cancer [12, 14]. Studies have also shown that dogs are good models for exposure to ionizing radiation, requiring similar doses to induce damage and "radiographic and histopathologic changes [17]."

A final advantage of using companion dogs as a research tool is animals live in the same environment as humans and are exposed to the same oncogenic factors [13-14, 16]. The initiation and progression of the tumors are subjective to the same environmental factors [12]. As seen in the mesothelioma example, a dog could be used as a sentinel to predict effects on humans before they arise due to the development of effects in the companion animal. Studies on early indicators of cancer are being done in dogs such as urine, growth factors, and treatment [13]. Similar to humans, as canine life expectancies increase, owed to improved nutrition, vaccinations, and health care, the incidence of cancer in the species increases [12]. Due to all the reasons given above, a dog provides an ideal model for a comparison to human effects due to ionizing radiation.

1.4 Objectives and Overview

In an effort to fill the void concerning the effects of low doses of radiation, an extensive model will be developed comparing canine radiation doses to that of human radiation doses from CT. Until 2008, no canine dosimetry software existed [18]and to date no physical canine phantoms have been made for determining radiation doses to dogs from external beam irradiation. With a standard model in place, a large cohort of dogs could be followed and the doses from CT compared to the incidence of cancer in dogs. The cancer risks to the canine species could then be translated to humans with an appropriate model.

The tissue weighting factors for CT in a dog is hypothesized to be comparable to those of a human child, and doses to specific organs in a dog can be compared to doses of analogous organs in a human. The theory, that a close relationship between doses in a human child and canine organs exists, was tested by building a canine anatomic physical phantom from tissue-equivalent substances then measuring dose to the brain while in the primary beam, and dose from secondary scatter to the brain when the chest of the phantom was in the primary beam. Doses were then compared to a human model. The canine species was found to be a reasonable model when used to ascertain the stochastic effects of CT.

The specific goals of this project were to (1) begin developing a canine phantom, (2) collect dose data to the brain of the dog phantom, and (3) use the analysis as a guide to better develop technique in the future. Tissue equivalent substances (TES) were used to build a phantom that was employed to measure canine dose and available for use in future studies. The equivalent dose to the brain was found utilizing three different scan parameters. A final goal was to compare canine dose data to a human model using the same parameters. The analysis helped determine efficient methods to build a model and develop recommendations for future study in this area.

CHAPTER 2

MATERIALS AND METHODS

2.1 Creation of the Physical Canine Anatomic Phantom

A phantom was created by combing transverse slices of tissue equivalent substances from the superior end to the inferior end of a dog. The CT scan used to develop the phantom was that of a male foxhound, specimen H07233 – ED7, on the GEMINI TruFlight Big Bore PET/CT (Phillips Healthcare Cleveland, OH) installed at VTH. There were a total of 725 slices at two millimeters each which were later combined to make 290 five-mm slices.

After the CT scan was complete, the data were transferred to Eclipse Treatment Planning software (Varian Medical Systems Inc. 2006 Palo Alto, CA) where the individual organs could be viewed and contoured. The locations of the organs were outlined on each slice. The chosen organs were: adrenals, brain, lens of the eye, gall bladder, heart, intestine (large and small combined), kidneys, liver, lungs, pancreas, red marrow, skeleton, skin, spleen, stomach, testicles, thyroid, trachea, and urinary bladder. Each of these organs corresponds to an organ typically used for human dose assessments. Organs were identified by comparing the CT images to a canine anatomy book [19] with final approval of organ dimensions and location completed by a board certified veterinary radiologist. Figure 3 shows an example of the Varian software with the organs of interest contoured.

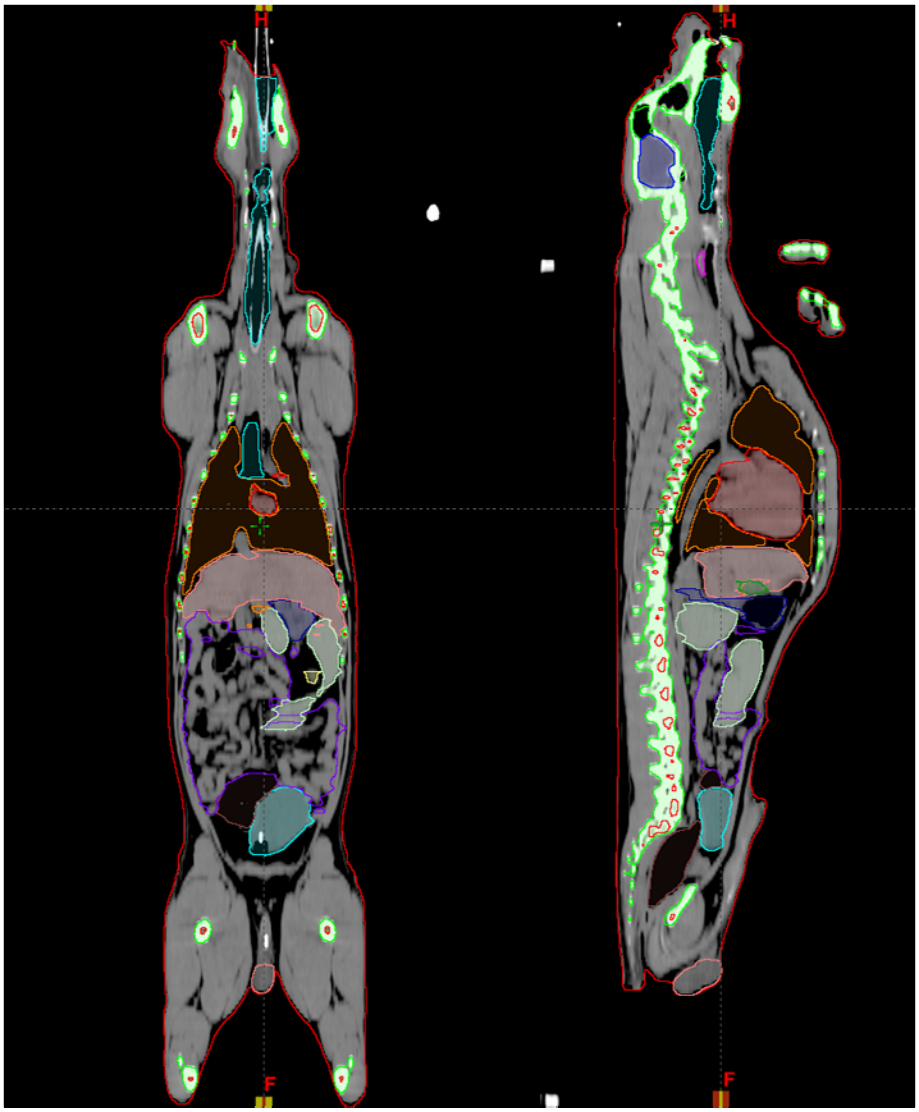

Figure 3: A frontal and sagittal view of the CT of specimen H07233-ED7 with organs of interest contoured.

After contouring all the organs of interest, each slice was printed at full size with a one cm grid (1) on paper to make a book for use as a reference and (2) on a transparency to be attached to a tissue-equivalent slice. Each printed slice utilized a reference number correlating the distance from an assigned centerline and also color-coded the outlines of the organs. When it was necessary to repeat colors, the organs chosen were distanced from each other so as to prevent confusion. The organs and their corresponding colors are listed in table 1.

Table 1: Organs of interest and the corresponding identifying color.

Organ	Color
Adrenals	Dark Green
Brain	Blue
Eye Lenses	Brown
Gall Bladder	Dark Green
Heart	Red
Intestine	Purple
Kidneys	Yellow
Liver	Pink
Lungs	Orange
Pancreas	Brown
Red Marrow	Red
Skeleton/Bone	Green
Skin	Red
Spleen	Light Green
Stomach	Dark Blue
Testicles	Pink
Thyroid	Magenta
Trachea/Air	Blue
Urinary Bladder	Cyan

The transparencies also functioned as a method of identifying the individual types of tissues in the slices during the construction process. Each tissue type was shaded a different color on the transparency, as listed in Table 2, which allowed a clear line to remove sections of the soft tissue equivalent substances (STES) slices that would be replaced by the appropriate substance. An example slice with the bone locations removed is exhibited in figure 4. Slices were carved using a hooked utility knife along the external contour lines from the CT image to give realistic dimensions to phantom with the slice number labeled on the edge of the slice in ball point pen.

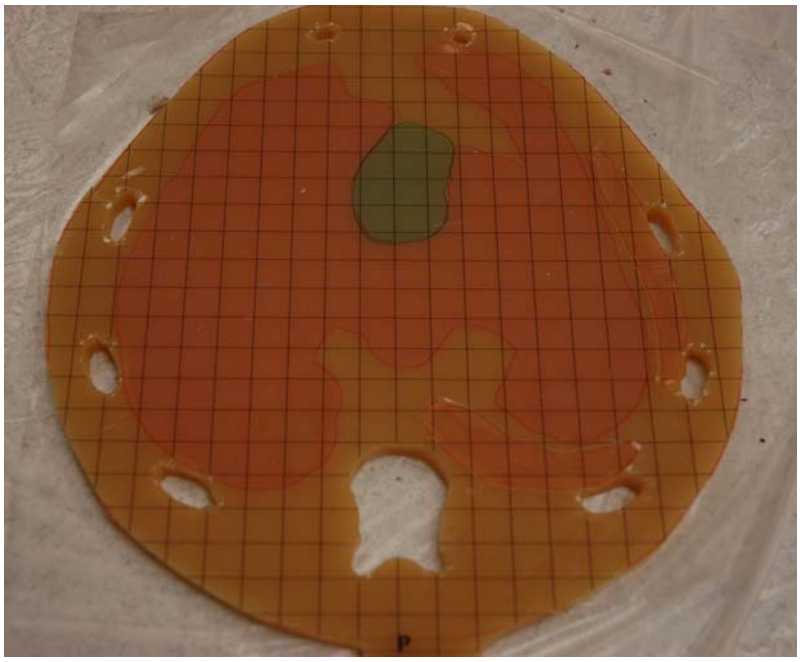

Figure 4: A soft-tissue equivalent slice with a transparency attached. Voids have been made in the soft tissue for the bone. The other colors on the transparency indicate the locations of other organs. Orange at the bottom right is lung tissue that was later removed and filled with LTES. The dark green and pink indicate the gall bladder and liver respectively that remain for dose assessments.

Table 2: Tissue type with corresponding color on transparencies and recipe.

Tissue type	Color	Recipe
Soft tissue	Transparent leaving tan STES color	Smooth-On equal parts A and B with 2.8% calcium carbonate [20]
Bone	Green	Bone Meal and Pieces in Epoxy
Lung	Orange	Soft tissue recipe with 10:1 micro-beads [20]
Airway	Blue	Remove all TES and left exposed

2.2 Construction of the Tissue-Equivalent Substances

2.2.1 Soft Tissue-Equivalent Substance

Each slice was created as uniform sheet in a mold attached to a transparency. There were two molds made of wood with an opening 30.5 cm by 26.5 cm and five mm deep. An additional four

molds were made out of carbon fiber (30.5 cm × 26.5 cm × 4 mm). The total interior volume necessary to fill the molds was calculated and converted to a mass of the STES using a density of one g/cm^3 to get an approximate volume to fill the mold. The recipe used for the STES was based upon a paper from Winslow et al. [20] with equal parts of A and B of the Smooth-On PMC 121/30 Dry Polyurethane rubber compounds (Smooth-On Inc., Easton, PA) and 0.028% calcium carbonate ($CaCO_3$) (Acros Organics, Thermo Fisher Scientific, Fairlawn, NJ). The total mass for each part was 264 grams and 15 grams of $CaCO_3$. All mass measurements were made using nutritional scales Model 3833 Serial Number 4409 V0427 (Taylor Precision Products, Oak Brook, IL). The scale measures one gram graduations, so all amounts were rounded to the nearest whole number.

It was important to ensure enough bowls, spoons, and molds were clean and the buckets of the Smooth-On were opened before beginning the slice pouring. Batches of six slices were made in each session. Materials prepared in advance included the $CaCO_3$ which was measured out in small bowls. Part B was likewise prepared in large mixing bowls, shown in figure 5. The $CaCO_3$ was combined with part B and mixed with a Chefmate 5-speed Electric hand mixer model HM-3000 (Target Corporation, Minneapolis, MN) for at least 1 minute or until most of the $CaCO_3$ was dissolved. The bowl was set aside to allow bubbles to rise to the top. The bowls were allowed to sit for approximately 10 minutes while the molds were set up for the pouring process.

Figure 5: Part B (left), $CaCO_3$ (center), Part A (right) poured and measured in mixing bowls with scales.

Each mold was set up in a station to include all the necessary items for pouring the slices. Wax paper was used under the slices to create a barrier between the STES and the counter-top. A mold was placed on top of the wax paper with a transparency, weight and press board nearby to be added on top of the STES (figure 6). Large smooth cutting boards were used as press boards and full buckets of the Smooth-On were used as large weights to go on the press boards. Small weights were used to hold the mold in place while the STES was poured. A needle and toothpicks were readily available for popping bubbles that were formed during the pouring process (figure 6).

Figure 6: Mold setup (left) with wax paper under a carbon fiber mold with small weights on the mold and a full box of Smooth-On in the background. Bubbles are being popped in fresh STES with a toothpick (right).

Part B and $CaCO_3$ were mixed again by hand and the remaining bubbles at the surface were popped with a toothpick after all materials had been assembled. Part A was poured into the bowl with part B and $CaCO_3$ while on the scale. The compound was hand mixed with a kitchen spoon to reduce the number of bubbles and then set aside. The mixture had a low viscosity when first mixed, so it was allowed to cure for a few minutes to allow viscosity to increase. Increased viscosity mixtures better suspend any un-dissolved $CaCO_3$. The STES was then poured into the mold, and the mixture spread. The bubbles were again popped on the surface of the STES and the transparency was carefully laid face up starting at one end of the mold while

pressing the transparency down to prevent air pockets from forming as seen in figure 7. If bubbles did develop they were removed by piercing the transparency with a needle. On top of the transparency, a press board was placed with weights to force excess mixture out of the mold (Figure 7).

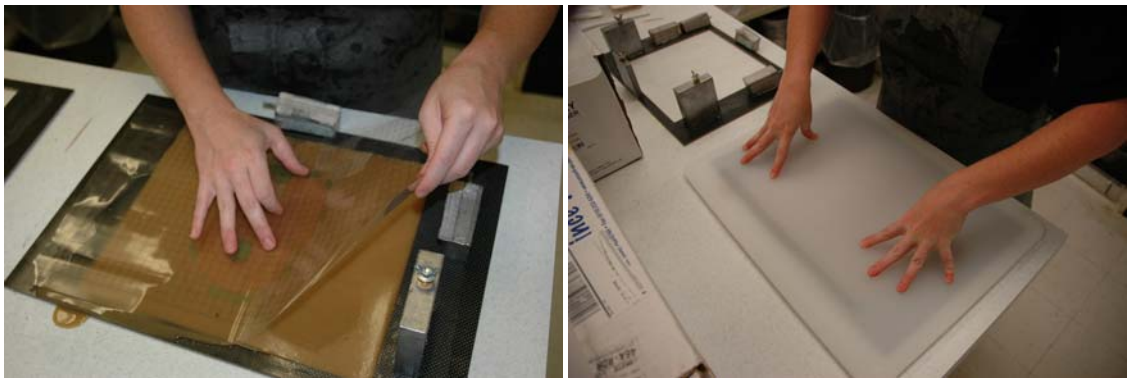

Figure 7: A transparency being laid on uncured STES (left) and a press board used to remove excess STES (right).

Each station consisted of all the materials necessary to produce one slice. From the bottom up the materials are: wax paper, mold, STES mixture (Part B, $CaCO_3$, and Part A), transparency, press board and weights. The cycle described above to complete a slice station was continued for all six stations. At the end of each slice pouring session, it was important to close part A and B buckets tightly.

For all new measurement was made the scales were zeroed and separate spoons were used to mix each combination of ingredients. The spoon used to stop flow from the part A bucket, as it was being poured on to the scale, was not used to mix any other compound in order to prevent cross contamination. Also, it was critical to remove the wax paper from the back of the slices in 3 to 4 hours after pouring (Figure 8) and the slices and excess compound removed from the molds. The slices were laid transparency down on the counter top to prevent the rubber from adhering to the laminate. However, the bowls and spoons were allowed to sit 24 hours to let the compound completely cure before removing the rubber (Figure 8). Once the slices were

cured, a hooked-blade utility knife was used to carve along the outlines of the bone indicated on the transparencies to remove the STES. Each slice was fitted with a sheet of contact paper on the opposite side of the transparency over empty spaces to be later filled with bone equivalent tissue.

Figure 8: Wax paper being removed from partially cured STES (left) and fully cured STES being removed from mixing bowl (right).

2.2.2 Bone Equivalent Material

Bone equivalent material was created and placed in the appropriate sections removed from the STES slices (figure 4). The bone equivalent material was produced using actual canine bones crushed and ground in a soil mill. Bone meal in the form of powder and bone pieces less than five mm diameter were produced from the bones. The bones were acquired through CSU anatomy lab. The anatomy lab obtained bones from a local humane society. Individual approval for use in research was not necessary per the Colorado State University Institutional Animal Care and Use Committee (IACUC) *Policy on the Use of Euthanized Animals for Tissue, Organs, or Other Parts* which states:

> "The distribution of whole animals or body parts from the Anatomy Lab for the purposes of student labs, continuing education courses, or for research does not require IACUC approval since the original acquisition of those animals required IACUC approval."

The bone meal and pieces were combined in different proportions to produce a compound with an appropriate density and scattering properties within an epoxy. The two part epoxy was combined first then the meal and pieces added in to create a coarse paste that could be pressed into the appropriate spaces in the STES slices.

Five trial mixtures were prepared with different mass proportions of bone meal and bone pieces with the epoxy compound. The epoxy compound chosen and proportions used are similar to those used in other studies of tissue-equivalent substances [20-21]. An initial epoxy base of 7 grams of Araldite GY 6010 (Huntsman Advanced Materials Americas Inc., The Woodlands, TX) and 3 grams of Jeffamine® T-403 (Huntsman Advanced Material Americas Inc., Conroe, TX) were mixed. Incremental amounts of bone meal and bone pieces were added to this base and placed in separate slots in the experimental slice for the density comparison (figure 9).

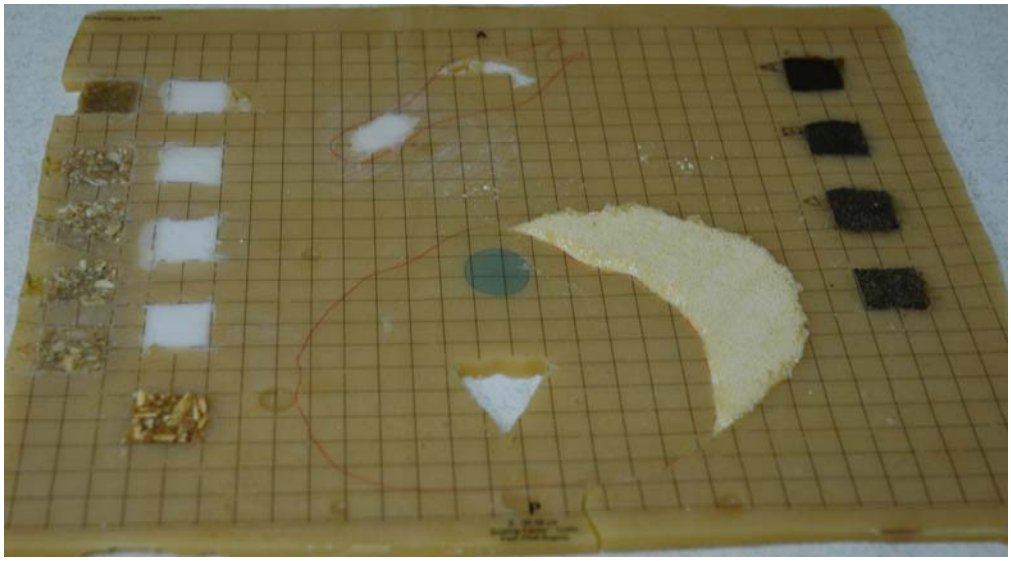

Figure 9: The test sheet for bone equivalent materials and lung tissue-equivalent substances. On the far left of the sheet is the bone equivalent material test slots I-V. Other test slots can be seen that were used to test other recipes that were unsuccessful.

The slots were labeled in Roman numerals I – V. The contents of each slot are listed in table 3. The first slot was filled with 10 grams of the base epoxy plus 10 grams of the bone meal. With the remainder of the mixture, 10 grams of bone pieces were added and slot II was filled. For slot

III, another 10 grams of bone pieces were added to the base left from the previous slot. The mixture for slot IV was the remainder of the mixture from slot III plus 5 grams of bone meal. Slot V had an additional 5 grams of bone meal added to the base.

Table 3: Contents of Test Slots for Bone Equivalent Material

I	II	III	IV	V
10 g epoxy compound (7 g Araldite, 3 g Jeffamine)	Remainder of I	Remainder of II	Remainder from III	Remainder from IV
10 g bone meal	10 g bone pieces	10 g bone pieces	5 g bone meal	5 g bone meal

The epoxy mixtures were allowed to cure for 48 hours then the test slice was scanned on the GEMINI TF PET/CT at a standard scan protocol of 120 kVp with 300 mAs. The scan was viewed on the Eclipse software where the Hounsfield units for the mixtures at various locations could be determined. A Hounsfield unit (CT number) is a quantitative number that is displayed on a reconstructed CT image [2]. The Hounsfield number is normalized using the linear attenuation coefficients ($\mu_{(x,y)}$) of the pixel before conversion of the image and the linear attenuation coefficients ($\mu_{(water)}$) of water. Hounsfield units can be calculated using the following equation:

$$CT(x,y) = 1{,}000 \cdot \frac{\left(\mu_{(x,y)} - \mu_{(water)}\right)}{\mu_{(water)}}$$

Hounsfield units range from -1,000 to 3,000. The linear attenuation coefficient is a function of the density of a material and density increases the probability of Compton interactions. Compton scattering is dominate at the average energies CT instruments operate. Therefore, Hounsfield units are a useful tool in understanding the physical properties of a substance [2] as they are calculated from the linear attenuation coefficients. The Hounsfield unit was used as a metric for the validity of a mixture as a bone equivalent material. The results of the bone analysis are listed in Chapter 3.

The final mixture for the bone equivalent material consisted of 20 grams epoxy mixture (14 grams Araldite and 6 grams Jeffamine®), 20 grams bone pieces, and 34 grams bone meal. Several batches of this mixture were made to fill the bone spaces in the phantom STES slices. During the construction process, the temperature of the room was 74 degrees Fahrenheit (23 °C) and 31 percent relative humidity. Once the epoxy cured for 48 hours, the bone was a hard substance with ridges that exceeded the five mm slice; thereby making each slice slightly thicker than five mm. These ridges were filed flush with the STES with a metal file, and the contact paper was removed from the back of the slices.

A canine skull, seen in figure 10,was used for the bone in the head, while the soft tissue and lung were fabricated from a recipe developed by Winslow et al. at the University of Florida [20]. The soft tissues surrounding the skull for the head were created using a euthanized canine head to make a mold. The cranium of a hound was acquired from the CSU anatomy lab; therefore, as with the bones separate approval through IACUC was not necessary.

Figure 10: The skull used for bone in the construction of the head for the phantom.

The ears were removed from the head, and it was placed in a vacuum sealed bag and frozen. A rubber mold was created of the head by pouring a mixture of the two parts of Smooth-

On around the frozen head that was perched on a stand made of plastic in a cardboard box. The rubber mold mixture was allowed to cure overnight then the mold was cut in half and the vacuum sealed dog head removed. After the skull was stripped of fur and soft tissue, it was placed inside the mold to be integrated into the structure of the phantom (figure 11). The mold was coated with cooking spray, and the skull was suspended using small strips of previously cured STES to provide a space between the bone and the edge of the mold, allowing STES to flow around the skull. The spacers allowed the skull to be coated with STES and remain suspended while the rubber cured. Once the STES had cured around the skull, it was removed from the mold (figure 11) and excess material was shaved off the phantom head using a utility knife. The phantom head was then matched up to the slices starting at the neck.

Figure 11: Canine skull inside mold before and after STES is added.

2.2.3 Lung Tissue-equivalent Substance

The lung tissue equivalent substance (LTES) was manufactured in the same manner as the STES. A premeasured amount of calcium carbonate was placed in a small bowl (0.028 % of total) with equal parts of part A and B of Smooth-On. Part B was first mixed with the calcium carbonate using the mixer for at least one minute. Bubbles were allowed to rise then popped with a toothpick, followed by mixing in part A. A ten to one ratio by mass of Poly-fil polystyrene micro-beads (Fairfield, Danbury, CA) were added to the base to make an adhesive paste that would

stick to gloves and other surfaces. The paste was pressed into the previously contoured spaces cut out of the STES slices. Great care was takes to keep the thickness of the slices at five mm by using the smooth hard edge of a ruler to push substances above the five mm away from the slice. Then, the press boards and weights used in manufacturing the STES were placed on top of the slices to be removed in three to four hours.

2.3 Dose Measurements to the Canine and Human Brain

All CT scans utilized an identical procedure, as described in this section. A CT series consisted of a two-view pilot scan followed by full scans at 90, 120, and 140 kVp at 300 mAs/slice. First, the 0.125 cc PTW N31005 ion chamber, serial number: 0709 (Freiburg, Germany), was securely placed in the region of the dog brain and attached to the Keithley 35050A Dosimeter, serial number: 69696 (Cleveland, OH). The dog and dosimeter were positioned on the CT gantry with foam cushioning beneath the head and body (when included) for stabilizing purposes. The dosimeter measured picoCoulombs. The dosimeter and ion chamber were calibrated as a system at the University of Wisconsin – Madison Department of Medical Physics Accredited Dosimetry Calibration Laboratory (UWM-RCL). Calibration was compliant with the ISO/IEC 17025:2005 standards and UWM-RCL is accredited by the American Association of Physicists in Medicine and the American Association for Laboratory Accreditation. Calibration was completed February 23, 2011. Relative humidity and temperature were measured using an Abbeon indicator model M2A4 (Abbeon Cal, Inc., Santa Barbara, CA). Temperature and humidity were measured adjacent to the scanner. The gantry was adjusted to the correct setting for the part of the body to be scanned. The ion chamber was zeroed to prepare for the first scan before leaving the suite.

CT parameters were selected and recorded in the control room. A two-view pilot scan was then preformed. The charge collected by the ion chamber was recorded and the ion chamber

zeroed for the next scan. The time of day for the entire series was noted during the pilot scan. CT parameters were adjusted for the next scan and the process repeated. At the end of the series, the temperature, humidity and a background charge were taken. The ion chamber charge was read and instrument reset between each scan. The gantry had to be reset and the exposure series was repeated after each series of CT scans.

Data for the barometric pressure during scans were collected from the Fort Collins Weather Station located on CSU campus northwest of the Lory Student Center and available online. The barometric pressure, measured in milibars, was read off graphs (available in Appendix B) using the time of the corresponding scan. The following pressure conversion was used to change the data from millibars to millimeters of mercury (mmHg):

$$P_{\text{mmHg}} = 0.750062 \cdot P_{\text{millibars}}$$

A temperature and pressure correction was necessary for each scan series as an open air ion chamber was used. The calibration factors were normalized to 1 atmosphere (760 Torr) at 22°C. The correction factor ($C_{T,P}$) was computed with the following expression:

$$C_{T,P} = \frac{273.15 + T}{295.15} \cdot \frac{760}{P}$$

For standard conditions T is temperature measured in °C and P is the pressure in Torr (mmHg). Ambient temperature of the CT suit was measured °F then converted to degree Celsius using the following conversion:

$$T_{^\circ C} = \frac{5}{9} \cdot \left(T_{^\circ F} - 32 \right)$$

As humidity has a near constant effect on ion chamber performance between 15% and 80% relative humidity, no corrections were made, but the humidity of the CT suite was monitored during the study [22].

The amount of kinetic energy released in matter is quantitatively known as Kerma (K). Incident photons or other ionizing radiation transfer kinetic energy to charged particles through photoelectric effect, Compton scattering or pair production [2]. Kerma is expressed in energy released in Joules per mass in kilograms. When energy is deposited in low z materials (air, water, and tissue), the kerma and absorbed dose are approximately equal. The absorbed dose is defined as the energy deposited in Joules per unit mass of material in kilograms. Both quantities are defined therefore by J/kg, also known as gray (Gy). Absorbed dose is useful as a tool to understand the amount of energy a tissue has absorbed and can be directly linked to the risks associated with ionizing radiation.

All radiation does not impart the same type of damage to a cell or tissue, therefore radiation weighting factors (w_R) have been developed to better characterize the biological effects of ionizing radiation. The International Commission on Radiological Protection (ICRP) has established w_R factors and most recently published them in ICRP 103. The ICRP recommends the use of a radiation weighting factor of one for photons, electrons and muons [23]. Radiation weighting factors are multiplied by the absorbed dose to yield the quantity known as equivalent dose. The unit associated with equivalent dose is the Sievert (Sv). The equivalent dose to the canine phantom brain was calculated using the following equation:

$$H = Q \cdot \text{System Coef.} \cdot C_{T,P}$$

The previously defined temperature and pressure correction factor is $C_{T,P}$, Q is charge in picoCoulombs (pC) and the system coefficient was defined when calibrated as 2.433×10^{-4} Gy/Rdg. The generic unit for the read-out of a system is Rdg. The Rdg unit used is the pC readout, effectively giving a calibration coefficient of Gy/pC. All equivalent doses were converted to mGy for convenience.

Shrimpton and Jones developed a program (ImPACT CT Patient Dosimetry Calculator version 1.0.2 using NRPB-SR250 data) to calculate human doses to organs from a CT using 23 different exposure settings relevant to 27 models of CT scanners [24]. The program utilizes Monte Carlo techniques applied to an anthropomorphic mathematical phantom to produce dose data, normalized to unit tissue doses, to 27 organs. The program uses standard scan parameters as inputs in the model and generates the equivalent and effective doses to each of the specified organs and a total effective dose to the patient. An option in the program allows the user to specify either ICRP 103 or ICRP 60 tissue weighting factors. All data for this study was produced using ICRP 103 tissue weighting factors.

The ImPACT calculator was utilized as a means of developing dose data to a human equivalent to the CT scan performed on the canine phantom by selecting the same scan parameters. The dose to the brain, total dose to the body and the CT dose index (CTDI) information was collected for each of the selected kVp settings (90, 120, and 140). The model parameters employed are listed in table 4. The calculated human dose to the brain was then compared to the measured dose to the canine phantom.

Table 4: Parameters applied to ImPACT model for dose generation for kVp and mAs effects analysis.

Primary Beam Location	Head	Chest	Head
Manufacturer	Philips	Philips	Philips
Scanner	Philips Big Bore	Philips Big Bore	Philips Big Bore
kV	90,120,140	90,120,140	120
Scan Region	Head	Body	Head
Start Position	72	48	72
End Position	94	70	94
Organ Weighting scheme	103	103	103
Tube current	300	300	100,200,500
Rotation time	1	1	1
Spiral pitch	1	1	1
Collimation	16 × 0.75	16 × 0.75	16 × 0.75

The data sets measured were dose to the canine phantom when (1) the head was in the primary beam and (2) the chest was in the primary beam. Each data set was split into two groups using a random sequence generator. Dose comparisons were performed on the head and chest in the primary beam for the canine data and adult or child doses to determine if any relationship existed. Splitting data for comparison allowed each group of dog data to have unique statistical analysis. Group one, consisting of data points 1, 2, 6, 7, 8, 12, and 13, was assigned to the adult dose comparison when the head was in the primary beam. Group two, consisting of data points 3, 4, 5, 9, 10, 11, and 14, was assigned to the child dose comparison when the head was in the primary beam. Group three, consisting of data points 3, 4, and 5, was assigned to the adult dose comparison when the chest was in the primary beam. Group four, consisting of data points 1 and 2, was assigned to the child dose comparison when the chest was in the primary beam. The grouping is demonstrated in Figure 12.

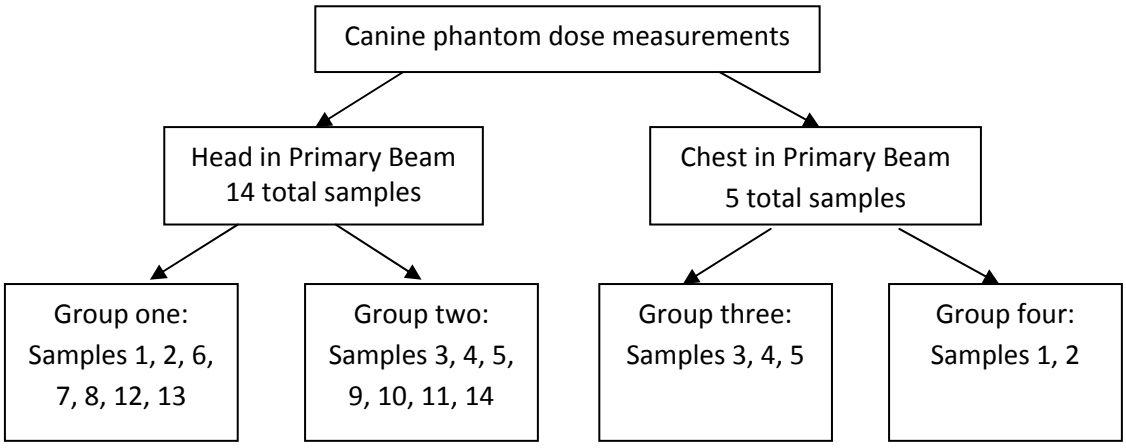

Figure 12: A pictorial representation of the grouping of data for statistical analysis between measured canine doses and generated human doses.

The dose comparisons were done comparing the expected dose to the human generated from the ImPACT software to the ratio of the measured dose in the canine phantom to the expected dose to the human. The ratio was:

$$R = \frac{\text{Dose to Canine}}{\text{Dose to human}}$$

A polynomial fit was then made to the data and an R squared valued determined using Microsoft® Excel software. The results of this analysis are presented in chapter 3. An average ratio of the doses was derived with a standard deviation to better understand how the dog and human doses relate.

CHAPTER 3

RESULTS

3.1 Bone Equivalent Material

Hounsfield units were collected at several random positions in the bone equivalent material generated with bone meal, bone pieces and epoxy. Results of the Hounsfield units for slot I-V and the final compound are shown in Table 5. All the average Hounsfield units were above 400 with the lowest at 423 and the final compound with the highest at 823. A wide range is seen in each bone test slot with standard deviations ranging from 173 to 319. A more detailed view of the data collected is given in Appendix C.

Table 5: Mean, standard deviation, maximum and minimum Hounsfield units at various locations in each test slot and in the final compound for bone equivalent material.

Slot	I	II	III	IV	V	Final
Mean	**423**	**522**	**527**	**576**	**770**	**894**
STDEV	176	245	194	173	284	319
Maximum	791	1228	899	828	1385	1591
Minimum	173	329	127	360	323	486

3.2 Dose Comparisons

Equivalent doses were measured to the brain of the canine phantom and recorded. A full report of the data is in the appendix with a summary reported as a mean with a standard deviation, variance and range in Table 6.

Table 6: Mean, Standard Deviation, Variance and Range of equivalent doses (mSv) to the brain at each kVp setting due to the head and chest in the primary beam.

	Head			Chest		
	90 kVp	120 kVp	140 kVp	90 kVp	120 kVp	140 kVp
Mean	12.957	32.798	49.237	0	1.963	2.715
Std Dev.	0.452	0.771	0.873	0	2.715	0.424
Variance	0.204	0.594	0.762	-	0.063	0.180
Range	12.3-13.9	31.9-34.9	48.3-51.1	0	1.68-2.29	2.21-3.32

Expected doses to a ten year old child most closely matched the measured doses to the canine phantom when the head was in the primary beam. The primary beam comparison for the adult and the child are in Figure 13. The mean value of the ratio (± standard deviation) for the child was 0.95 (± 0.12) which is not significantly different from 1 (t = 1.10; df = 6; $P > 0.05$) whereas the mean ratio for the adult predicted dose was 1.24 (± 0.15) which is statistically significantly greater than 1 (t = 4.23; df = 6; $P < 0.01$).

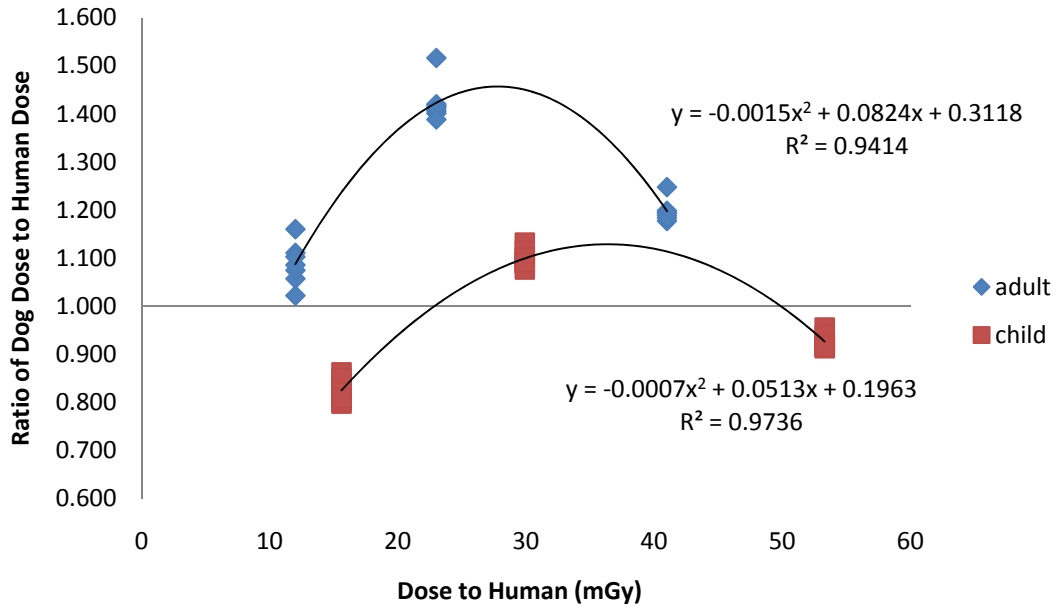

Figure 13: Comparison of expected doses to a human (adult and child) to the ratio of the dog dose to the human (adult or child) when the head is in the primary beam.

The comparison of the doses to the brain with the chest in the primary beam yielded more variable results (Figure 14). Mean (± standard deviations) ratios for both child and adult were 3.34 (± 2.93) and 3.99 (± 3.35), respectively, and ratios ranged from less than one to greater than five.

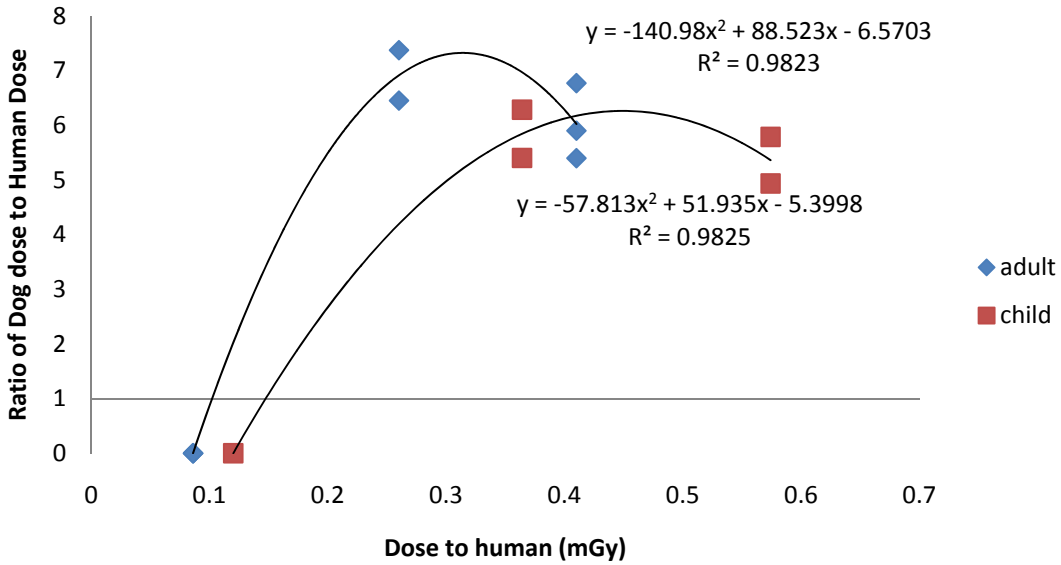

Figure 14: Comparison of the expected doses to a human (adult and child) to the ratio of the measured dog dose to the human dose (adult or child) when the chest is in the primary beam.

All five of the dose measurements for the scatter to the brain from the chest in the primary beam at 90 kVp were 0.000 pC. To establish the validity of such results a test was performed to ascertain the probability of five readings at zero when the actual result should be non-zero. As the premise assumed equal probability of zero or non-zero values, the probability was calculated with the following expression:

$$P(y) = \frac{1}{2^n}$$

The probability of y successful trials in n number of trials with y and n both equal to five was 0.03125.

A comparison of the change in dose due to an incremental change in the product of the tube current and the rotation time measured in mAs was completed as a verification of the instrumentation (CT scanner and detection equipment). The measured doses are given in Table 7 for each mAs.

Table 7: Doses in mGy from various mAs at 120 kVp

mAs	Dose (mGy)			
100	9.454	9.483	9.492	8.260
200	19.329	19.488	19.332	19.434
300	29.291	-	-	-
500	48.141	48.576	48.692	47.823

A linear model was placed on the data and found to be not statistically different. The comparison can be seen in Figure 15.

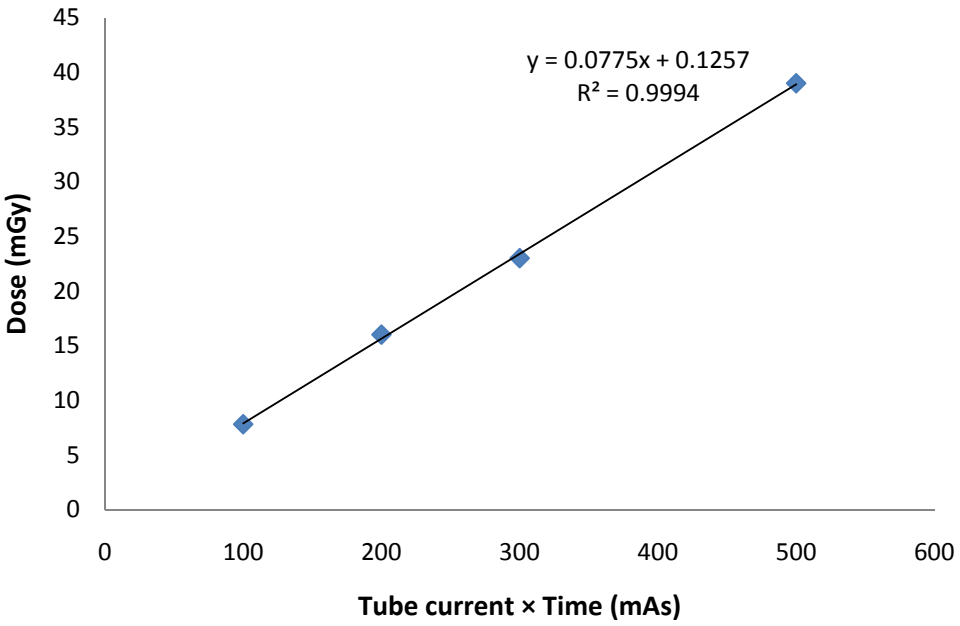

Figure 15: Comparison of measured dose to canine phantom brain when in the primary beam from incremental increases in the tube current-rotation time product (mAs).

CHAPTER 4:

DISCUSSION

4.1 Creating the Physical Canine Anatomic Phantom

A full body scan from a research dog already being studied was used to prevent unnecessary irradiation of an animal while developing a method to create a phantom made from individual slices. Also, scanning a research dog removed any privacy issues with pets and their owners.

Organs of interest were chosen for the dose to be measured in these specified organs in the phantom then compared to the doses of a human model. Time constraints restricted study to only the brain but all the chosen organs were identified and contoured. The organs chosen corresponded with ICRP 103 organs which were assigned a radiation weighting factor [23]. The female organs were excluded along with a few other organs that were not present (thymus) or too difficult to contour (salivary glands, breast, oesophagus, extra thoracic region, lymphatic nodes, muscle, and oral mucosa) since the scanned dog was male.

Errors arose when the placement of the organs was not clear because the organs were identified from the CT scans. The contrast was low surrounding some organs which made outlining the organs difficult. Estimates were made when organ locations were identified.

4.2 Error and Difficulty Associated with the Construction of the Phantom

4.2.1 Soft Tissue-equivalent Substance

STES slices need to be exact in thickness to prevent elongation of the phantom dog. Maintaining exact slice thickness was a difficult process. The system of pressing out excess mixture with weights was helpful to provide a smooth surface to both sides of the slice, but it was found that the STES could not be completely pressed away from the mold adding about 0.5-1 mm to the slice thickness. The carbon fiber molds better maintained slice thickness at five mm. An additional four carbon fiber molds were made in addition to the original two wooden molds in an effort to expedite the phantom building process. If the excess STES was not removed completely, the mold would be thicker; therefore, the slices would also be thicker. Much care was taken after each slice was completed to clean the mold, however some residue remained and the slices were slightly thicker than five mm at times. The entire phantom length was increased by approximately four cm which increased the amount of tissue available to scatter the radiation. However, this extra tissue equivalent material was not a concern since it was distributed throughout the length of the phantom and variability among dogs exceeds this amount.

The STES was mixed in large plastic and metal mixing bowls with rubber spoons that afforded easy clean up after the mixture had cured. The individual constituents of the rubber compound were difficult to clean, but when mixed properly the rubber would easily pull from most plastic, metal or rubber surfaces. The mixture was not easily removed from wood, laminate, or carbon fiber unless removed within four hours of mixing. The wax paper placed between the mixture and the countertop offered an easy removal system and a smooth surface for the completed slices as long as the wax paper was removed from the slices within four hours of pouring. If allowed to remain on the STES during the complete curing process the wax paper

was difficult to remove and left large amounts of residue. The STES adhered to the molds after curing which required energy, time and strength to remove. Large amounts of time were spent cleaning the molds, bowls and spoons in order to complete the project, however if cleaned at appropriate times the total time and necessary energy required was reduced.

One attempt was made to reduce time for mixing by making a double batch of STES and pouring it into two molds. This method was ineffective as it was difficult to determine the amount of STES necessary to fill the mold, leaving too little to fill the second mold.

A major benefit of tissue-equivalent substances is the workability and flexibility in form that allows any structure to be built then used for dose assessments. The tissue-equivalent substances used have additional benefits of closely matching the scattering properties of tissue over a large range of energies [20-21]. The tissue-equivalent substances for lung and soft tissue were effective and convenient. The density for STES and LTES were previously calculated at 1.04 g/cm^3 and 0.33 g/cm^3, as were the average Hounsfield units at 9.8 and -678.4, respectively [20].

Calcium Carbonate ($CaCO_3$) did not easily dissolve into the Smooth-On mixture. Small amounts of the $CaCO_3$ powder settled to the bottom of the STES slice during construction and remained there as the slice cured. Every five mm there was a speckled layer of denser calcium carbonate that was clearly visible to the naked eye when viewing the slices, but these speckles of $CaCO_3$ were not significant on the CT scans. These speckles did not appear to impact the study.

4.2.2 Bone Equivalent Material

The bone tissue-equivalent substance (BTES) recipe from Winslow et al. and Jones et al. was not reproducible when attempted. The epoxy resin base would not produce a mixture that was workable in the laboratory. Liquid portions were not sufficient to suspend the proportions of powder called for in the recipe. The mixture would remain a powder regardless of the amount

of mixing or heating that was suggested by the authors and other parties through personal communication. A number of different combinations of heating the constituents, changing the order the substances were added, and changing proportions of liquid constituents to powders were tried, but the mixture would not combine. It was decided the recipe is not fit for high altitude mixing and an alternative method of using real bone was devised. The final method was selected due to the density, Hounsfield unit and workability of the materials. The test slots of bone meal and bone pieces all had an average value above 400 Hounsfield units and ranges within the accepted values of 400 to 1000 [20] as seen in Table 5. The wide variety of density is expected within a test slot as the bone equivalent material included a mixture of bones from real dogs. The bone equivalent material showed the variation seen in real bone tissue due to the different types of bones. The two major types of bone are the high density cortical bone, and the less dense trabecular bone[25].

The ears were removed from the head to better simulate a therapy session since the ears are often tied back. The molding process was made easier by reducing the extra flesh and fur of the ears. The first attempt to create a mold for the canine head was using plaster of Paris. The head was not vacuum sealed at the time but the fur was covered with petroleum jelly to keep the plaster from matting in the fur. Unfortunately, the plaster did not cure successfully because the flesh kept the plaster of Paris moist. The head was later vacuum sealed in a bag to prevent the mold material from getting matted in the fur.

Air bubbles and pockets were a concern. After the mixture was poured into the molds, the STES was allowed to sit for a few minutes so the bubbles could rise to the top. Bubbles were then popped using a toothpick. Care was taken to remove all the bubbles, but due to the nature of the materials (i.e. material set-up too quickly, bubbles would not pop) some air pockets remained. Air bubbles were created in the bone equivalent material as it was placed in the STES

slices. Bubbles did not rise as the viscosity was high in the bone equivalent material. Special care was taken not to create air pockets; however, some were created and could not be removed. The LTES mixture adhered to the utensils and gloves which made it difficult to spread and pour without producing air pockets. The air pockets in all of the tissue equivalent substances could change the scatter or absorption of the x-rays, but the effect was small. The air in place of tissue reduced the amount of x-rays scattered or absorbed, thereby reducing the measured dose. The error associated with the air-filled ion chamber was greater than that of the micrometer sized bubbles, and the error of the ion chamber was small at 1.9% [22].

4.3 Dose Measurements and Calculations

The original goal of the project was to determine a resultant overall dose and dose to each organ of interest, but due to time constraints this was not achievable. The construction of the physical canine anatomic phantom required more time than anticipated with only six slices being made at a time. The construction of the bone equivalent material took significant time as a new recipe had to be developed and tested before the phantom could be completed. The time required to take scans is not long for data collection, but set up can be time consuming. Availability of CT equipment is restricted due to relatively high patient and study volume. Another time constraint is due to tube loading. As the CT is used heat builds in the tube. The amount of heat built up in the tube must remain below certain levels in order for the instrument to operate without damage to the CT tube. The number of consecutive scans is limited by tube use.

Air kerma was measured at one point in the brain. Future studies would benefit by determining the dose at various locations in the organs to better characterize the dose to the organ. Absorbed dose and kerma vary due to distance from the surface of the tissue. Kerma decreases linearly with greater depth in tissue whereas absorbed dose reaches a peak

somewhere below the surface then decreases linearly with increasing depth [25]. Kerma measured at the center of the organ may not be the best estimation of dose to the entire organ.

Measured dose to an organ may vary considerably if measured in through different methods. Future research in this area would benefit from a more comprehensive look at the dose to various points in the organ. A method that would bring more comprehensive dose results would be to use thermoluminescent dosimeters (TLD) placed at numerous locations in the organs. The TLDs could then be read and averaged much like the CTDI. TLDs are commonly used in dose assessments in phantoms when the equipment and time is available[26]. The ion chamber method used provided the dose to one point in the organ which was approximately the middle of the brain. It was efficient because it provided quick and accurate results without having to remove the detector between scans.

Background doses were considered insignificant, with all background measurements reading 0.000 pC except one. The one exception could have been the result of the movement of the instrument which caused a collection of charge. Background doses were not included in calculations. One reason for the low background is the shielding for the PET/CT suite is encompassing which prevents outside (natural background) from entering the room. The room is well ventilated so background from radon is also low and not expected to result in a dose.

For the analysis of the data, two dose collection sets were gathered to give data on dose when the detector is in the primary beam and dose from scattered radiation when the detector is not in the primary beam. The two different configurations better characterize a clinical situation where a subject (human or animal) would receive dose from scatter and from a primary beam.

The ratio of the doses was an indicator of how well the expected dose for the human matched the measured dose for the canine. A ratio of one would indicate a close match and the

variability from one would indicate a discrepancy. The ratio of 0.95 ± 0.12 suggests expected doses to a ten year old child's brain most closely follow the measured values for the canine phantom when the detector was in the primary beam.

Additional research needs to be completed with respect to the radiation scattered from the primary beam to other parts of the body to best characterize the relationship between the total effective dose to a child and the dose to the phantom. No preliminary indication that the response of the canine phantom does not statistically differ from that of a human model when using the ten year old child data with the detector in the primary beam. However, analysis does suggest a statistically different value in the dog dose to the brain due to scatter from a body scan than for a human at any age, but the values were highly variable. Body orientation, mass or bone structure may account for this variability.

An interesting factor that arose was the null reading for scatter dose to the phantom brain from the 90 kVp setting. The statistical possibility of this being an error was low at 3.125 percent. The repeated null readings may be due to the nature of the energies scattered, and their ability to penetrate into the skull. The scatter at 90 kVp would be another point of interest for future research.

The results of the mAs study was a good confirmation of equipment performance. The results showed a linear response to the increase in mAs. A developed scaling factor can be used for any kVp to adjust the dose in relation to mAs. The linear response is expected as an increase in tube current or the time the tube is on will produce a larger number of photons. The mAs affects only the quantity of photons in the beam not the quality of the photons.

CHAPTER 5

CONCLUSIONS

A portion of a physical canine anatomic phantom was built using a previously developed soft tissue-equivalent substance, lung tissue-equivalent substance and a new bone equivalent material in 140 transverse slices. The new bone equivalent material was tested for response to x-ray radiation using a Hounsfield unit comparison and was found to fall within acceptable ranges of 400 to 1000. A separate phantom head was created that contained an ex-vivo skull and used for dose measurements to the brain of a dog from a CT scanner.

Preliminary data of the equivalent dose to the canine phantom brain indicates a good fit, To the generated dose from the human model, to a ten year old human child under similar CT scan parameters when the detector is in the primary beam with a mean ratio (± SD) of 0.95 (± 0.12). The adult generated dose was not found to be a good fit for the canine data with a mean ratio of 1.24 (± 0.15). Insufficient data was available to characterize a relationship between the canine dose and the human (child or adult) dose when the brain and detector were not in the primary beam. The knowledge acquired in the process of building the phantom and collecting data can be used as a pilot to future studies in developing a better canine model for translational research in low dose studies from Computed Tomography.

It is well documented that not all tissues respond to radiation the same with many exhibiting different sensitivities. The ICRP developed new tissue weighting factors (w_T) to estimate the detriment to a particular tissue in ICRP 103. The product of the tissue weighting

factors and the equivalent doses to the respective organs summed over the whole body gives the effective dose. Effective dose, like equivalent dose, is expressed in Sieverts (Sv). Equivalent dose of only one organ (the brain) was calculated. Once more data is acquired from the entire canine phantom and tissue weighting factors for dogs established; a total effective dose for a dog can be calculated. The future of this research lies with developing a model that relates the CT parameters to a total effective dose to a dog with canine equivalent tissue weighting factors. It may also be useful to take dose measurements at other facilities across the country to characterize the effect the instrument has on the dose. The dog dose model could then include the average doses from a number of facilities.

An additional future path of this research includes a large scale study of canine CT doses performed on animals treated at numerous institutions by utilizing the large amount of dogs imaged for non-cancer related reasons at facilities like Colorado State University. Data could be collected for the dose dogs receive then followed into the future for cancer incidence. A translational model would then be produced to better aid in translational research that directly links the dose to organs in a dog to the dose in a human using the parameter canine model and the canine cancer incidence data. Useful studies relating cancer incidence to low doses in dogs, which live on a shorter time scale, could then be dose which will shed light on effects of low doses of radiation to humans.

REFERENCES

1. National Council on Radiation Protection and Measurements. and National Council on Radiation Protection and Measurements. Scientific Committee 6-2 on Radiation Exposure of the U.S. Population., *Ionizing radiation exposure of the population of the United States : recommendations of the National Council on Radiation Protection and Measurements*. NCRP report. 2009, Bethesda, Md.: National Council on Radiation Protection and Measurements. xv, 387 p.

2. Bushberg, J.T., et al., *The essential physics of medical imaging*. 2nd ed. 2002, Philidelphia: Lippincott Williams & Wilkins. 933.

3. Shrimpton, P.C. and S. Edyvean, *Commentary: CT scanner dosimetry.* The British Journal of Radiology, 1998. **71**: p. 3.

4. McCrohan, J.L., et al., *Average radiation doses in a standard head examination for 250 CT systems.* Radiology, 1987. **163**(1): p. 6.

5. Smith, A., G.A. Shah, and T. Kron, *Variation of patient dose in head CT.* The British Journal of Radiology, 1998. **71**: p. 1296-1301.

6. Huda, W., *Dose and image quality in CT.* Pediatric Radiology, 2002. **32**(10): p. 709-13; discussion 751-4.

7. NRC, *Stochastic effects - Glossary definition*, U.S. NRC, Editor. 2011, NRC: Washington D.C.

8. National Research Council (U.S.). Committee to Assess Health Risks from Exposure to Low Level of Ionizing Radiation., *Health risks from exposure to low levels of ionizing radiation : BEIR VII Phase 2*. 2006, Washington, D.C.: National Academies Press. xvi, 406 p.

9. Khanna, C., et al., *Guiding the optimal translation of new cancer treatments from canine to human cancer patients.* Clin Cancer Res, 2009. **15**(18): p. 5671-7.

10. Cohen, B.J. and F.M. Loew, *Laboratory Animal Medicine: Historical Perspectives in Laboratory Animal Medicine*, ed. J.G. Fox, B.J. Cohen, and F.M. Loew. 1984, Orlando, FL: Academic Press, Inc.

11. Shearin, A.L. and E.A. Ostrander, *Leading the way: canine models of genomics and disease.* Dis Model Mech, 2010. **3**(1-2): p. 27-34.

12. Paoloni, M. and C. Khanna, *Translation of new cancer treatments from pet dogs to humans.* Nat Rev Cancer, 2008. **8**(2): p. 147-56.

13. Knapp, D.W. and D.J. Waters, *Naturally occurring cancer in pet dogs: important models for developing improved cancer therapy for humans.* Mol Med Today, 1997. **3**(1): p. 8-11.

14. De Vico, G., et al., *Spontaneous Tumours of Pet Dog as Models for Human Cancers: Searching for Adequate Guidelines.* Rivista Di Biologia, 2005. **98**(2): p. 279-296.

15. University of California, S.F.I.A.C.a.U.C., *Normative Values: The Dog*. 2004.

16. Mueller, F., B. Fuchs, and B. Kaser-Hotz, *Comparative biology of human and canine osteosarcoma.* Anticancer Res, 2007. **27**(1A): p. 155-64.

17. Fike, J.R., et al., *Radiation dose response of normal brain.* Int J Radiat Oncol Biol Phys, 1988. **14**(1): p. 63-70.

18. Padilla, L., et al., *Canine anatomic phantom for preclinical dosimetry in internal emitter therapy.* J Nucl Med, 2008. **49**(3): p. 446-52.

19. Stanley, D., et al., *Color Atlas of Veterinary Anatomy: The dog and cat*. Second ed. Vol. 3. 2009, Philidelphia, PA: Mosby Elsevier.

20. Winslow, J.F., et al., *Construction of anthropomorphic phantoms for use in dosimetry studies.* J Appl Clin Med Phys, 2009. **10**(3): p. 2986.

21. Jones, A.K., D.E. Hintenlang, and W.E. Bolch, *Tissue-equivalent materials for construction of tomographic dosimetry phantoms in pediatric radiology.* Med Phys, 2003. **30**(8): p. 2072-81.

22. UW-RCL, *Report of Calibration for Diagnostic Ionization Chamber and Electrometer System*. 2011, Medical Radiation Research Center: Madision, WI.

23. ICRP, *The 2007 Recommendations of the International Commission on Radiological Protection.* Ann ICRP, 2007. **103**.

24. Shrimpton, P.C. and D.G. Jones, *Normalised organ doses for x-ray computed tomography calculated using monte carlo techniques and a mathematical anthropomorphic phantom.* Radiation Protection Dosimetry, 1993. **49**(1): p. 241-243.

25. Cember, H. and T.E. Johnson, *Introduction to health physics*. 4th ed. 2009, New York: McGraw-Hill Medical. xi, 843 p.

26. Huang, B., M.W. Law, and P.L. Khong, *Whole-body PET/CT scanning: estimation of radiation dose and cancer risk.* Radiology, 2009. **251**(1): p. 166-74.

APPENDIX A

NCRP 160 Effective Dose Data

Collective effective dose (S), effective dose per individual in the U.S. population (E_{US}), and average effective dose for the exposed group (E_{Exp}) for 2006.

Exposure Category	S (person-Sv)	EUS (mSv)	EExp (mSv)
Ubiquitous background	933,000	3.11	3.11
Internal, inhalation (radon and thoron)	684,000	2.28	2.28
External, Space	99,000	0.33	0.33
Internal, ingestion	87,000	0.29	0.29
External, terrestrial	63,000	0.21	0.21
Medical	899,000	3.00	__[a]
CT	440,000	1.47	__[a]
Nuclear medicine	231,000	0.77	__[a]
Interventional fluoroscopy	128,000	0.43	__[a]
Conventional radiography and fluoroscopy	100,000	0.33	__[a]
Consumer	39,000	0.13	0.001 – 0.3[b]
Industrial, security, medical, educational and research	1,000	0.003	0.001—0.01[b]
Occupational	1,400	0.005	1.1
Medical	550		0.8
Aviation	530		3.1
Commercial nuclear power	110		1.9
Industry and commerce	110		0.8
Education and research	60		0.7
Government, DOE, military	40		0.6
Total	1,870,000[c]	6.2[c]	

[a]Not determined for the medical category because the number of patients exposed is not known, only the number of procedures.
[b]The range of values for the various subcategories in this category.
[c]Rounded values. Data adapted from NCRP 160

APPENDIX B

Barometric Pressure Data Plots

Fort Collins Weather Station Data Plots obtained to determine barometric pressure at time of scan. Measured in millibars then converted to millimeters of mercury (mmHg).
Conversion: $.750062 \text{ millibars} = 1 \text{ mmHg}$

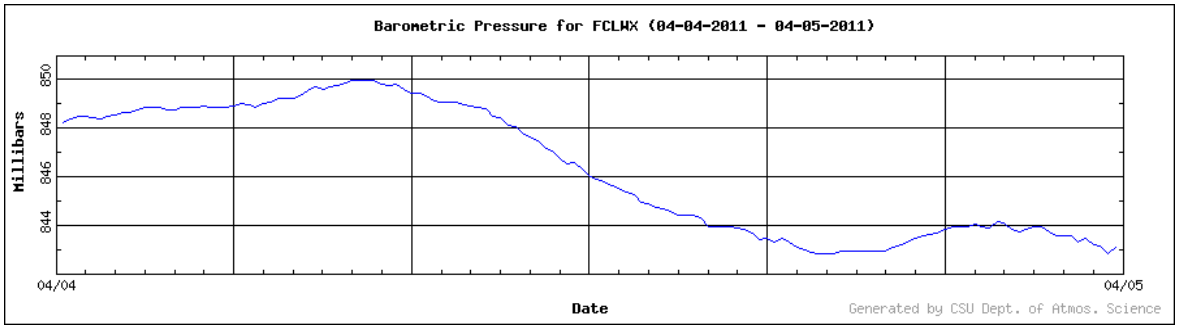

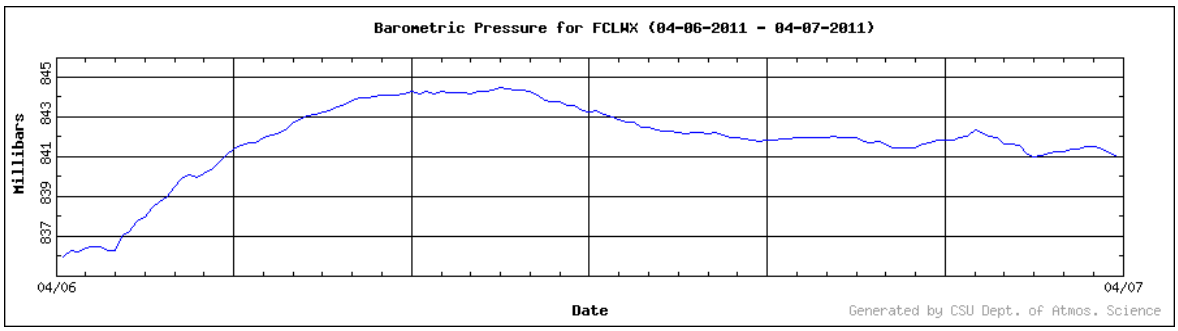

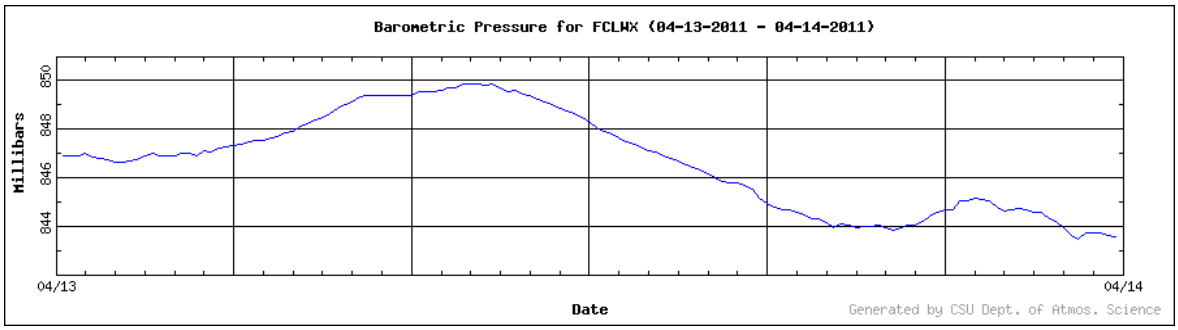

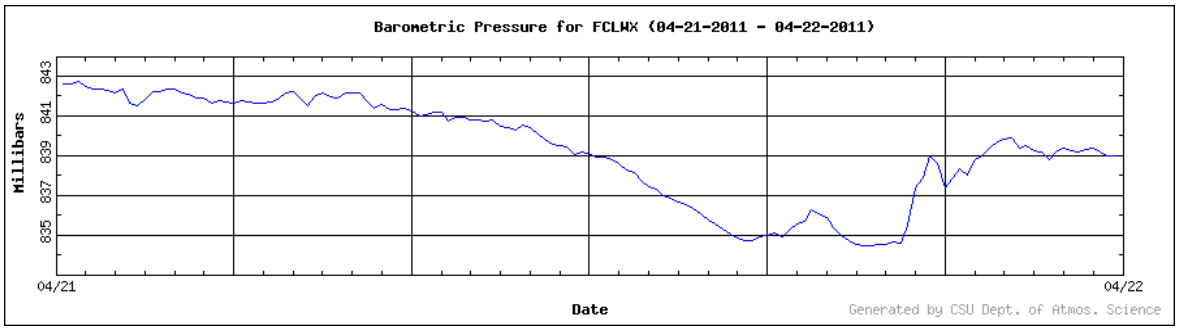

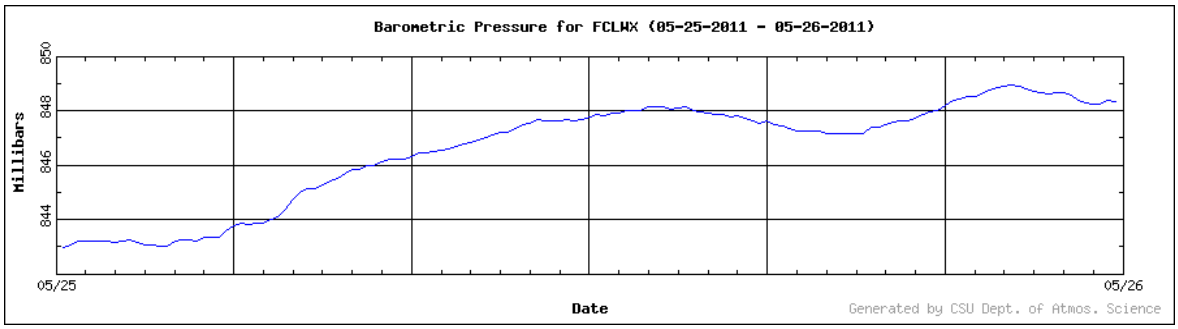
Barometric Pressure for FCLWX (05-25-2011 - 05-26-2011)
Millibars
850
848
846
844
05/25
05/26
Date
Generated by CSU Dept. of Atmos. Science

APPENDIX C

Hounsfield Unit Data for Bone Equivalent Material

Hounsfield units at various locations in each test slot and in the final compound for bone equivalent material.

Slot	I	II	III	IV	V	Final
	456	522	605	613	1385	1111
	284	502	434	822	735	930
	530	363	534	682	492	1049
	173	424	635	828	520	1591
	791	413	603	681	806	827
	357	662	693	360	820	486
	459	598	511	406	856	676
	678	331	559	376	965	1240
	411	408	368	370	782	890
	272	480	899	463	323	517
	359	329	127	659	535	637
	311	1228	357	646	1021	771
Mean	**423**	**522**	**527**	**576**	**770**	**894**
STDEV	176	245	194	173	284	319
Maximum	791	1228	899	828	1385	1591
Minimum	173	329	127	360	323	486

APPENDIX D

Charge and Dose Data from CT scans of Physical Canine Phantom

Data collected from scans with the brain in the primary beam with information including charge (pC), barometric pressure (mbars), temperature (°F), percent relative humidity, and the time the scans were completed. The temperature correction factor is included as well as the mean, standard deviation, maximum and minimum for each category.

	Pilot (pC)	90 kVp (pC)	120 kVp (pC)	140 kVp (pC)	Background (pC)	Pressure (mbars)	Temperature (°F)	RH %	Time	C(T,P)
4/4/2011	0.44	47.9	120	176	0	849	72	31.5	830	1.194
4/6/2011	0.235	42.05	110.5	165.5	0	844.5	71		1000	1.198
4/13/2011-1	0.415	46.1	116	174.5	0	847	73	34.5	1330	1.199
4/13/2011-2	0.415	42.7	114.5	172	0.365	847	72	35	1340	1.197
4/13/2011-3	0.415	42.9	113	169	0	846.5	72	35	1350	1.198
4/13/2011-4	0.41	43.6	112	167.5	0	846.5	71	35	1400	1.196
4/21/2011-1	0.395	43.85	110	166.5	0	837.5	71	34	1330	1.208
4/21/2011-2	0.53	45.3	111	167		837	71	33.5	1343	1.209
4/21/2011-3	0.385	44.1	110.5	167		837	71	33	1350	1.209
4/21/2011-4	0.385	45.15	111	166		836.5	70	33	1358	1.208
4/21/2011-5	0.385	43.6	109.5	165.5	0	836.5	70	33	1407	1.208
4/21/2011-6	0.4	44.3	110.5	166.5	0	836	70	33	1419	1.208
4/21/2011-7	0.4	45	108.6	165	0	836	70	33.5	1430	1.208
4/21/2011-8	0.39	42.9	111	166		835.5	70	33.5	1442	1.209
Mean	0.40	44.25	112.01	168.14	0.04		71.00	33.65		1.204
Std Dev	0.06	1.55	3.02	3.50	0.12		0.96	1.03		0.006
Maximum	0.53	47.90	120.00	176.00	0.37	849.00	73.00	35.00		1.209
Minimum	0.24	42.05	108.60	165.00	0.00	835.50	70.00	31.50		1.194

Charge readings for scans with the head in the primary beam and the corresponding air kerma. The mean, standard deviation, maximum and minimum for each category is included.

	Pilot (pC)	90 kVp (pC)	120 kVp (pC)	140 kVp (pC)	K(air-pilot) (mGy)	K(air-90) (mGy)	K(air-120) (mGy)	K(air-140) (mGy)
4/4/2011	0.44	47.9	120	176	0.128	13.919	34.871	51.143
4/6/2011	0.235	42.05	110.5	165.5	0.069	12.261	32.220	48.258
4/13/2011-1	0.415	46.1	116	174.5	0.121	13.453	33.851	50.923
4/13/2011-2	0.415	42.7	114.5	172	0.121	12.437	33.351	50.099
4/13/2011-3	0.415	42.9	113	169	0.121	12.503	32.933	49.254
4/13/2011-4	0.41	43.6	112	167.5	0.119	12.683	32.581	48.725
4/21/2011-1	0.395	43.85	110	166.5	0.116	12.893	32.343	48.955
4/21/2011-2	0.53	45.3	111	167	0.156	13.327	32.656	49.131
4/21/2011-3	0.385	44.1	110.5	167	0.113	12.974	32.509	49.131
4/21/2011-4	0.385	45.15	111	166	0.113	13.266	32.614	48.774
4/21/2011-5	0.385	43.6	109.5	165.5	0.113	12.811	32.173	48.627
4/21/2011-6	0.4	44.3	110.5	166.5	0.118	13.024	32.487	48.950
4/21/2011-7	0.4	45	108.6	165	0.118	13.230	31.928	48.509
4/21/2011-8	0.39	42.9	111	166	0.115	12.620	32.653	48.833
Mean	0.40	44.25	112.01	168.14	0.117	12.957	32.798	49.237
Std Dev	0.06	1.55	3.02	3.50	0.018	0.452	0.771	0.873
Maximum	0.53	47.90	120.00	176.00	0.156	13.919	34.871	51.143
Minimum	0.24	42.05	108.60	165.00	0.069	12.261	31.928	48.258

Data collected from scans with the chest in the primary beam with information including charge (pC), barometric pressure (mbars), temperature (°F), percent relative humidity, and the time the scans were completed. The temperature correction factor is included as well as the mean, standard deviation, maximum and minimum for each category.

	Pilot (pC)	90 kVp (pC)	120 kVp (pC)	140 kVp (pC)	Background (pC)	Pressure (mbars)	Temperature (°F)	RH %	Time	C(T,P)
5/25/11-2	0.51	0	7.885	11.45	0	847	70	44	930	1.193
5/25/11-3	0.445	0	6.78	9.765	0	847	70	44	950	1.193
5/25/11-4	0.505	0	6.615	9.575	0	847.5	70	44	1030	1.192
5/25/11-5	0.52	0	5.785	8.37	0	847.5	70	44	1045	1.192
5/25/11-6	0.46	0		7.65	0	847.5	69	44	1055	1.190
Mean	0.488	0.000	6.766	9.362	0.000		69.800	44.000		1.192
Std Dev	0.033	0.000	0.864	1.456	0.000		0.447	0.000		0.001
Maximum	0.520	0.000	7.885	11.450	0.000	847.500	70.000	44.000		1.193
Minimum	0.445	0.000	5.785	7.650	0.000	847.000	69.000	44.000		1.190

Charge readings for scans with the chest in the primary beam and the corresponding air kerma.

	Pilot (pC)	90 kVp (pC)	120 kVp (pC)	140 kVp (pC)	K(air-pilot) (mGy)	K(air-90) (mGy)	K(air-120) (mGy)	K(air-140) (mGy)
5/25/11-2	0.51	0	7.885	11.45	0.148	0	2.288	3.323
5/25/11-3	0.445	0	6.78	9.765	0.129	0	1.967	2.834
5/25/11-4	0.505	0	6.615	9.575	0.146	0	1.918	2.777
5/25/11-5	0.52	0	5.785	8.37	0.151	0	1.678	2.427
5/25/11-6	0.46	0	-	7.65	0.133	0	-	2.214
Mean	0.488	0.000	6.766	9.362	0.142	0.000	1.963	2.715
Std Dev	0.033	0.000	0.864	1.456	0.010	0.000	0.251	0.424
Maximum	0.520	0.000	7.885	11.450	0.151	0.000	2.288	3.323
Minimum	0.445	0.000	5.785	7.650	0.129	0.000	1.678	2.214

Data collected from scans with the head in the primary beam at 120 kVP varying the tube current (mAs) with information including charge (pC), barometric pressure (mbars), temperature (°F), percent relative humidity, and the time the scans were completed. The temperature correction factor is included as well as the mean, standard deviation, maximum and minimum for each category.

	Pilot (pC)	100 mAs (pC)	200 mAs (pC)	300 mAs (pC)	500 mAs (pC)	Background (pC)	Pressure (mbars)	Temperature (°F)	RH %	Time	C(T,P)
5/25/11-1	0.505	32.6	66.65	101	166	0	847.5	70	44	1105	1.192
5/25/11-2	0.555	32.7	67.2		167.5	0	847.5	70	44	1130	1.192
5/25/11-3	0.535	32.75	66.7		168	0	848	70	44	1300	1.191
5/25/11-4		28.5	67.05		165		848	70	44	1320	1.191
Average	0.532	31.638	66.900	101.000	166.625	0.000		70.0	44.0		1.192
Std Dev	0.025	2.093	0.268		1.377						
Maximum	0.555	32.750	67.200	101.000	168.000	0.000					
Minimum	0.505	28.500	66.650	101.000	165.000	0.000					

Charge readings for scans with the head in the primary beam at a set 120 kVp while varying the tube current (mAs) and the corresponding air kerma.

	Pilot (pC)	100 mAs (pC)	200 mAs (pC)	300 mAs (pC)	500 mAs (pC)	K(air-pilot) (mGy)	K(air-100 mAs) (mGy)	K(air-200 mAs) (mGy)	K(air-300 mAs) (mGy)	K(air-500 mAs) (mGy)
5/25/11-1	0.505	32.6	66.65	101	166	0.146	9.454	19.329	29.291	48.141
5/25/11-2	0.555	32.7	67.2		167.5	0.161	9.483	19.488		48.576
5/25/11-3	0.535	32.75	66.7		168	0.155	9.492	19.332		48.692
5/25/11-4		28.5	67.05		165		8.260	19.434		47.823
Average	0.532	31.638	66.900	101.0	166.625	0.154	9.172	19.396	29.291	48.308
Std Dev	0.025	2.093	0.268		1.377	0.007	0.608	0.079		0.401
Maximum	0.555	32.750	67.200	101.0	168.000	0.161	9.492	19.488	29.291	48.692
Minimum	0.505	28.500	66.650	101.0	165.000	0.146	8.260	19.329	29.291	47.823